

Induction Hardening 5150 Steel: Effects of Initial Microstructure and Heating Rate

K.D. Clarke, C.J. Van Tyne, C.J. Vigil, and R.E. Hackenberg

(Submitted December 7, 2010)

Induction heating has permitted great progress in the surface hardening of a wide variety of steels, but results in a wide range of local thermal cycles. The metallurgical changes during rapid heating and cooling have not been sufficiently studied with respect to heating rate and prior microstructure. In the present investigation, induction dilatometry was performed on 5150 steel with ferrite-pearlite and tempered martensite initial microstructures to assess effects of experimentally controlled prior microstructure and heating rate on austenitization kinetics. Heating rates were varied from 0.3 to 300 °C/s to simulate industrial processes, and post-hardening metallography and hardness testing were performed. Results show that the transformation kinetics for prior ferrite-pearlite microstructures are significantly slower than for prior tempered martensite microstructures, although hardness is equivalent for a given thermal cycle. Metallographic evidence suggests significant remnant segregation of chromium in regions of pearlitic cementite (enriched); evidence of segregation was not observed metallographically for prior tempered martensite. Diffusion-based transformation simulations support observed ferrite-pearlite alloy segregation, suggest residual alloy segregation is possible for prior tempered martensite, and can be used to tailor austenitization thermal cycles to process requirements. Detailed time and temperature-dependent local microstructure development results from this study are directly applicable to practical induction hardening simulations.

Keywords austenitization, dilatometry, heating rate, induction heat treatment, steel, 5150

1. Introduction

Heat treatments to produce through-hardened 5150 steel entail austenitizing near 830 °C and oil quenching. Expected hardness is 55–60 HRC with slightly higher hardness possible at maximum specified carbon levels (Ref 1). Through-hardening

This paper is the 2010 HTS-Bodycote Best Paper in Heat Treating. The ASM Heat Treating Society established the Best Paper in Heat Treating Award in 1997 to recognize a paper that represents advancement in heat-treating technology, promotes heat treating in a substantial way, or represents a clear advancement in managing the business of heat treating. The award, endowed by Bodycote Thermal Process-North America, is open to all students, in full time or part-time education, at universities (or their equivalent) or colleges. It also is open to those students who have graduated within the past three years and whose paper describes work completed while an undergraduate or post graduate student. The subject matter of the paper is required to cover any aspect of research or development applied to the fields of heat treatment, surface engineering, hot isostatic pressing (hip), metallurgical coatings, testing, or materials processing, including any production process, information technology, or relevant management or business issues.

K.D. Clarke and C.J. Van Tyne, Colorado School of Mines, Golden, CO 80401; and **C.J. Vigil and R.E. Hackenberg**, Los Alamos National Laboratory, Los Alamos, NM 87545. Contact e-mail: kclarke@lanl.gov.

heat treatment times are designed to ensure sufficient time at temperature, and are thus relatively insensitive to prior microstructure. However, when 5150 is induction hardened, high heating rates result in significant prior microstructure effects (Ref 2, 3).

Induction heat treatments to produce surface hardening generate a wide variety of heating rates as a function of location. Therefore, detailed assessments of microstructural development as a function of heating rate and prior microstructural scale are critical. Most previous induction heat treatment studies have not quantitatively characterized prior microstructure and correlated results with measured heating rate. As a result, induction heat treatments and hardening processes are often designed based on experience and considerable experimental validation. For example, 5150 in the hot rolled (HR) condition is commonly subjected to a quench and temper (QT) prior to induction hardening. The prior QT treatment is said to reduce the required austenitizing temperature, improve case depth, increase maximum surface and average core hardness, raise the hardness slope in the case-core transition zone, improve compressive residual stresses, enhance repeatability, and remove microstructural banding (Ref 4). However, this extra heat treatment step may not always be necessary, and effects of the extra heat treatment on the above factors are not easily determined.

Ultimately, induction heat treatment design would be enhanced with a model that correctly correlates local time-temperature profiles with accurate microstructural development information, which would enable prediction of local material condition as a function of location. With such predictions, optimized induction heat treatments could be developed in short times to minimize processing and achieve tailored and

desirable final properties. The present study works toward this goal by evaluating the heating rate dependent response of HR and QT starting microstructures to provide microstructural development data as a function of heating rate for an induction hardening heat treatment.

2. Experimental Procedures

Table 1 presents measured and specified (Ref 5) compositions of the experimental material, with HR and QT starting microstructures shown in Fig. 1. The HR material is pearlite and ferrite with a hardness of 99 HRB. The QT material was produced by furnace heat treating HR material in the following fashion: austenitize for 1 h, oil quench, and temper for 1 h at 550 °C (37 HRC). Initial microstructural characteristics were measured, and are presented in Table 2 (Ref 6).

Induction dilatometry was performed on cylindrical samples 10 mm long and 3 mm diameter, using constant heating rates of 0.3, 3.0, 30, and 300 °C/s to a maximum temperature from 750 to 1200 °C in 25 °C increments. Heating was immediately followed by helium gas quenching to room temperature, achieving cooling rates of 250 °C/s (1100-800 °C) and

125 °C/s (800-500 °C). Transformation temperatures were determined from the dilation-versus-time data using a 0.0001 strain offset (Ref 7).

Final microstructures were evaluated using light optical (LOM) and scanning electron microscopy (SEM). The cylindrical dilatometer samples were mounted with the polish plane parallel to the longitudinal axis, then ground and polished to the axial center plane. Knoop (500 g) microhardness tests were performed according to ASTM E384 (Ref 8) and used to determine bulk hardness; reported Rockwell C (HRC) values were determined using ASTM E140 (Ref 9).

3. Results and Discussion

3.1 Dilatometry

Representative dilation strain versus temperature plots are presented in Fig. 2. Dilation response is highlighted in Fig. 2(a): on-heating (solid arrow) through A_{c1} and A_{c3} to the maximum temperature, followed by immediate quenching (dashed arrow) through M_s to room temperature. Deviations from the linear thermal contraction between maximum

Table 1 Measured and specified bulk composition of 5150 steel, wt.%

| Element | C | Mn | Cr | P | S | Si | Ni | Mo | Cu | Al |
|----------------------|-----------|-----------|-----------|------------|------------|-----------|-----------|-----------|-----------|---------|
| Tested material | 0.52 | 0.85 | 0.80 | 0.011 | 0.020 | 0.26 | 0.10 | 0.03 | 0.25 | 0.028 |
| ASTM A322-07 (Ref 5) | 0.48-0.53 | 0.70-0.90 | 0.70-0.90 | 0.035 max. | 0.040 max. | 0.15-0.30 | 0.25 max. | 0.06 max. | 0.35 max. | ... (a) |

(a) Killed steel is required

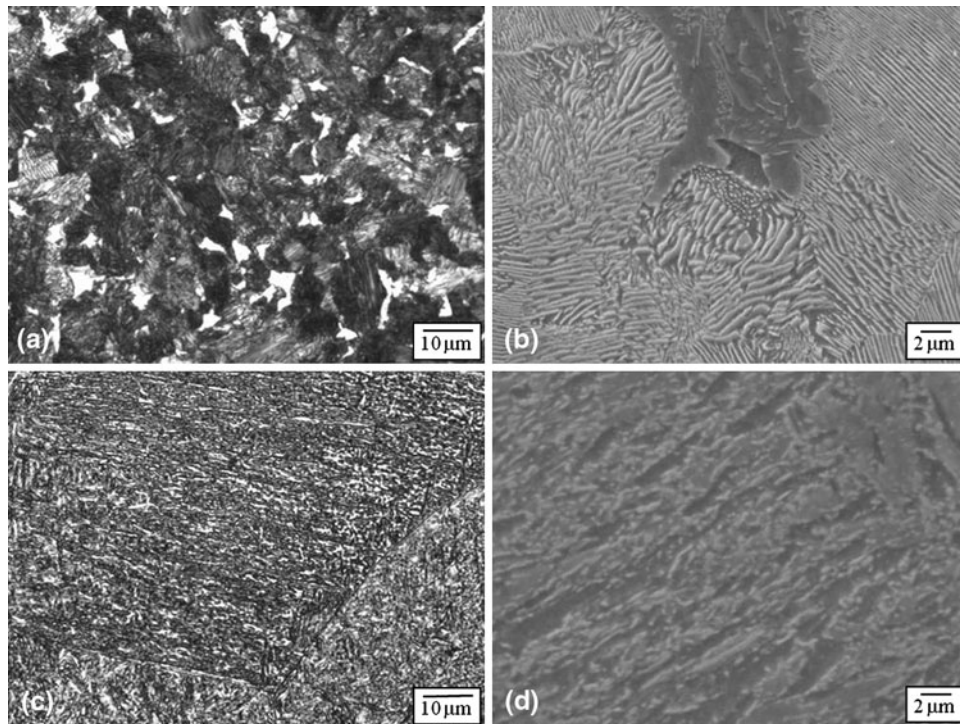


Fig. 1 Initial microstructures of the 5150 HR (a, b) and QT (c, d) materials. (a, c) optical, (b, d) electron micrographs

Table 2 Microstructural measurements of 5150 HR and QT materials

| Microstructural parameter | 5150 hot rolled | 5150 quench and tempered |
|---------------------------|--------------------|--------------------------|
| Pearlite | | |
| Lamellar spacing | 0.21 μm | |
| Colony size | 7.2 μm | |
| Carbide volume fraction | 0.084 | |
| Proeutectoid ferrite | | |
| Ferrite grain size | 2.4 μm | |
| Ferrite volume fraction | 0.076 | |
| Tempered martensite | | |
| Carbide size | | 0.12 μm |
| Carbide volume fraction | | 0.077 |

temperature and M_s indicate formation of non-martensitic transformation products (NMTP), including ferrite, pearlite, and/or bainite. With respect to induction hardening heat treatments, dilation response shows the effect of heating rate on austenite formation kinetics via $A_{\text{c}1}$ and $A_{\text{c}3}$, and can give evidence of the as-quenched austenite condition by showing substantial NMTP formation (low local hardenability) and giving M_s (primarily a function of austenite carbon content; Ref 10).

Figure 2(a) and (b) show the increase of $A_{\text{c}1}$ and $A_{\text{c}3}$ with increasing heating rate for the HR and QT material, respectively. Dilatometrically, no evidence of NMTP is found on-cooling, indicating sufficient local hardenability, and no systematic variation in M_s temperature with maximum temperature is found to imply a correlation with average austenite carbon content.

Figure 3(a) presents average $A_{\text{c}1}$ and $A_{\text{c}3}$ temperatures for the HR and QT material, respectively. Transformation temperatures increase with heating rate, and are higher for HR material in all cases. Figure 3(b) presents an (Fe + Alloying Elements)-C isopleth phase diagram calculated with Thermo-Calc[®], indicating $A_{\text{c}1}$ at approximately 730 °C. $A_{\text{c}1}$ is shown with a dashed line in Fig. 3(a), demonstrating that $A_{\text{c}1}$ for the HR and QT material is near the equilibrium value for a 0.3 °C/s heating rate. Figure 3(c) indicates increasing heating rate has a greater effect on transformation temperatures for HR material than for QT material. Increasing heating rate also has a greater effect on $A_{\text{c}3}$ than on $A_{\text{c}1}$. At 300 °C/s, $A_{\text{c}3}$ for the HR material is 40 °C higher than for the QT material, suggesting significantly slower austenitization kinetics.

3.2 Hardness

The primary goal of an induction hardening heat treatment is to produce hardened material, so as-quenched hardness was measured. Figure 4 presents hardness versus maximum temperature plots for HR and QT materials as a function of heating rate. For all heating rates, hardness increases with maximum temperature, and reaches a plateau of 60-61 HRC at a heating-rate-dependent threshold temperature. Neither HR nor QT materials show significantly higher maximum hardness. No quench cracking was found, except in material heated to 1200 °C at 0.3 °C/s.

For 300 °C/s cycles, 875 °C is required to achieve maximum hardness. Below 875 °C, hardness for 300 °C/s cycles is lowest for a given maximum temperature. When heated at 0.3 °C/s, maximum hardness is reached at 825 °C. Since

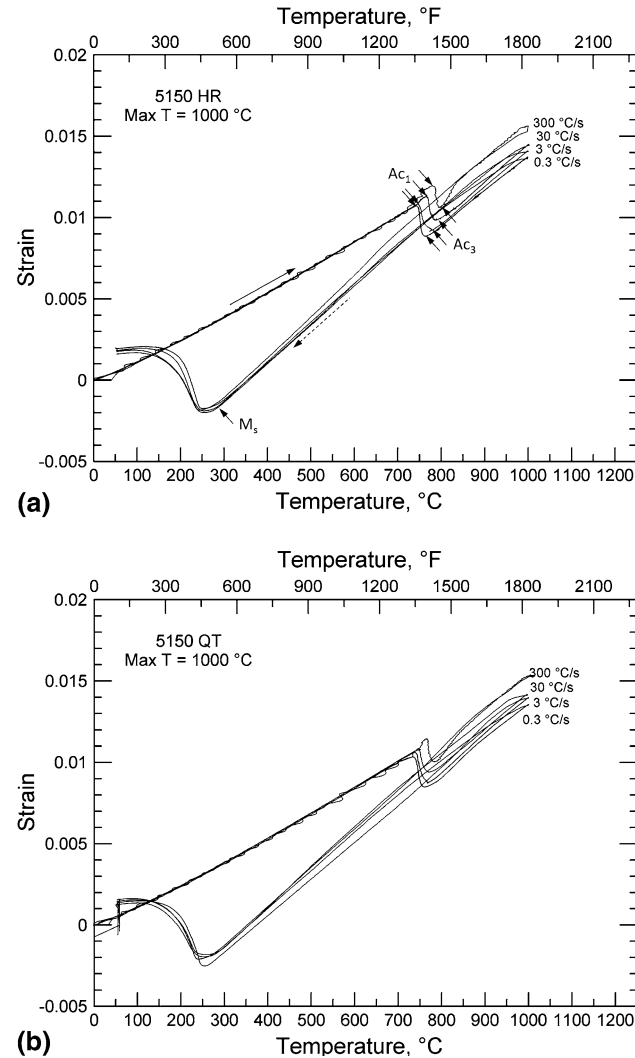


Fig. 2 Dilation vs. temperature curves for the 5150 (a) HR and (b) QT initial microstructures for indicated heating rates to a maximum temperature of 1000 °C

martensite hardness is predominantly a function of carbon content (Ref 11), hardness results suggest that, although austenite formation may be complete at much lower temperatures ($A_{\text{c}3}$ temperatures for HR and QT at 300 °C/s are 840 and 800 °C, respectively), the austenite does not attain maximum, homogeneously distributed carbon concentration until higher temperatures are reached. Based on hardness alone, the HR and QT materials appear to have a similar response for a given thermal cycle. Other factors, such as residual compressive stress levels at the surface of a real component, may result in higher measured surface hardness for prior QT steels. Separation of critical variables is imperative to understanding and simulating induction hardening heat treatments.

3.3 Microstructure

Although hardness results were similar, microstructural evaluation after quenching revealed significant differences in the heat treatment response of the two initial microstructures.

After induction heat treatment, all prior QT samples (not presented here) consisted of homogenous martensite, with fine

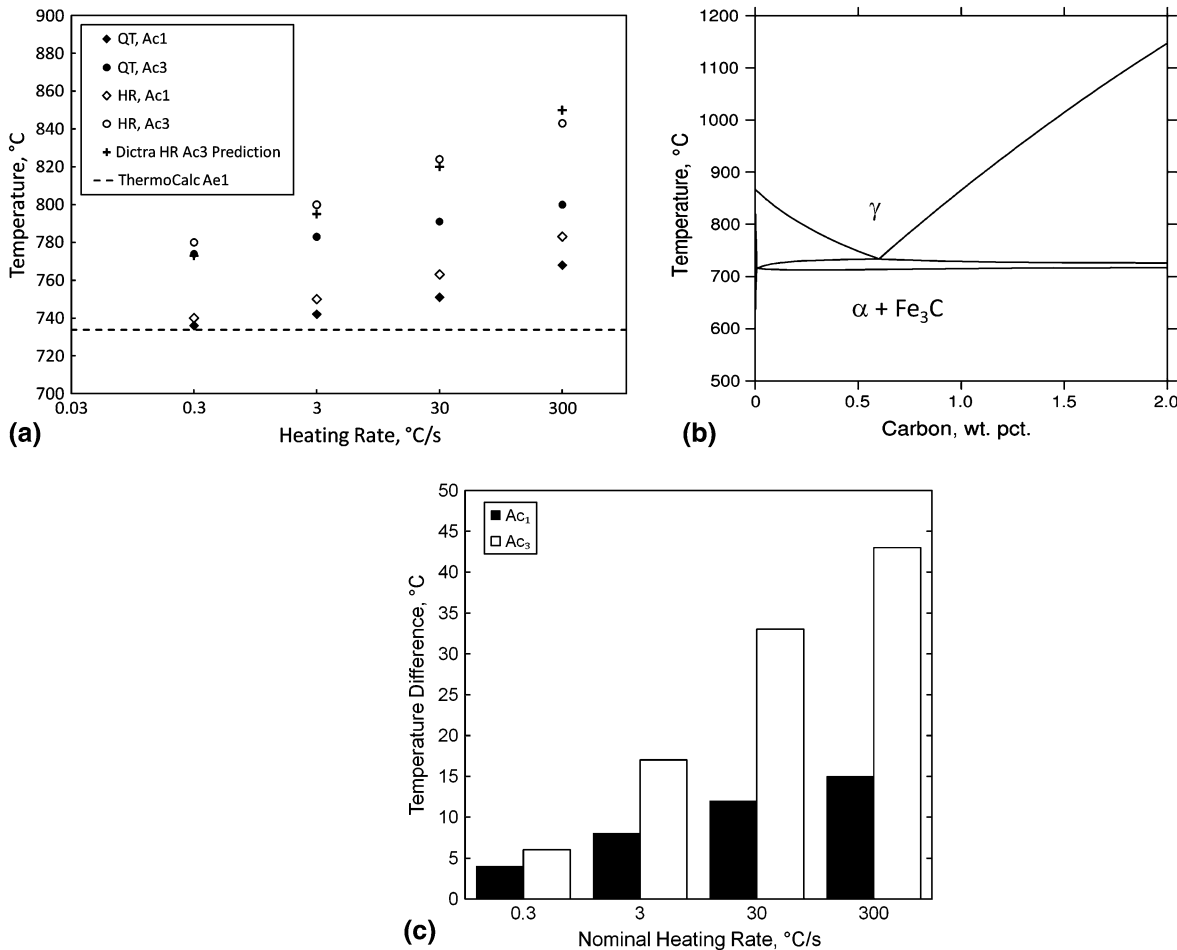


Fig. 3 (a) Summary of average A_{c1} , and A_{c3} temperatures from dilatometry for the HR and QT initial microstructures. (b) ThermoCalc[®] (Fe + M)-C isopleth for the experimental 5150 composition. (c) Temperature difference (HR-QT) between the A_{c1} and A_{c3} temperatures for each tested heating rate

tempered carbides (lower maximum temperatures) or carbide-free martensite (higher maximum temperatures). Cr and Mn slowed tempering kinetics of the initial microstructure, producing small, low-alloy carbides (Ref 11). The degree of prior tempering was not varied here, but changing tempering time-temperature combinations will change subsequent transformation kinetics.

The prior HR samples, however, revealed details of pearlitic carbide dissolution and proeutectoid ferrite transformation, providing insight into the austenitization process. Figure 5(a)-(c) present microstructures of samples heated at 30, 3, and 0.3 °C/s to 750 °C, just below, at, and just above A_{c1} for each respective heating rate (see Fig. 3a). Hardnesses are 23, 23, and 57.5 HRC, respectively. As expected, the 30 °C/s condition shows no evidence of austenite formation, Fig. 5(a). The 3 °C/s heat treatment shows some change in pearlitic carbide appearance, Fig. 5(b), but no hardness increase suggests no significant austenite formation. The 0.3 °C/s treatment produces martensite in prior pearlite regions and leaves much of the proeutectoid ferrite untransformed, Fig. 5(c). It has been shown that austenitization of ferrite-pearlite microstructures initiates in pearlite, followed by transformation of the proeutectoid ferrite regions (Ref 12). Some ferrite regions appear to have substructure that may indicate low-alloy, low hardenability

austenite was formed, and produced NMTP upon quenching (not detectable by dilatometry). Souza et al. (Ref 13) identified differential localized regions of hardenability due to Mn concentration variations.

Figure 6 presents micrographs of HR material heated at 30 °C/s to 775 °C, approximately 12 °C above A_{c1} (57 HRC). Figure 6(a) shows the majority of pearlite has transformed to austenite (now martensite), leaving some untransformed pearlite and proeutectoid ferrite, similar to Fig. 5(c). Transformation of pearlitic ferrite to austenite appears to proceed faster than dissolution of pearlitic cementite, which remains in the now martensitic regions in Fig. 6(b). Cementite remnants in martensite have previously been referred to as “pearlite ghosts” (Ref 14), and have been reported for induction hardened 5150 (Ref 15).

Figure 7 presents evidence of cementite remnants up to 1000 °C (arrows) for 300 °C/s treatments. While evidence at 1000 °C is subtle, apparent cementite remnants at 925 °C are 50 °C above the maximum hardness threshold temperature, which suggests full dissolution of carbides and maximum austenite carbon content. A possible explanation for cementite remnants after high temperature heat treatment is that Cr previously partitioned to pearlitic carbides did not diffuse sufficiently, which generates slightly different etching

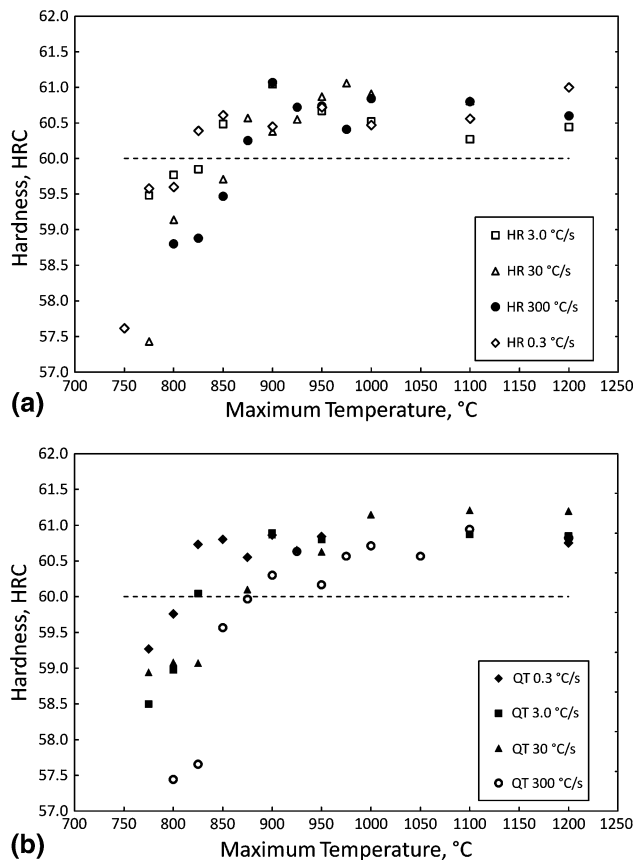


Fig. 4 Rockwell C hardness vs. maximum temperature for each heating rate. (a) HR and (b) QT initial microstructures

responses in high and low concentration regions, even though carbides were fully dissolved. Note that Mn or other alloying elements do not alter etching response like Cr, and may also have concentration gradients. Longer heat treatments may be necessary to eliminate segregation, because increasing temperature can promote austenite grain growth (Ref 15).

After austenite formation from prior ferrite, retained carbide dissolution is not controlled by carbon diffusion, but substitutional diffusion at interfaces, resulting in substitutional alloy gradients (Ref 14, 16). Previous induction hardening results (Ref 15) confirm remnant pearlite in 5150, but not in 1550 (no Cr). Similarly, no evidence of remnant pearlite was found in 1045 steel (no Cr), even after fast heat treatments only slightly above A_{c1} (Ref 17). No evidence of remnant pearlite is shown in Fig. 5(c) (0.3 °C/s to 750 °C), suggesting sufficient time for carbide dissolution and Cr diffusion and confirms that longer thermal cycles are less sensitive to prior microstructure and high temperature may not be necessary. It is unknown how prior QT treatments affect alloy segregation, but they are unlikely to eliminate composition gradients. Effects of chemical segregation on product performance are not currently understood, and may be especially important for fatigue initiation or wear performance. Bulk chemical banding could also affect local properties, as it is reported (Ref 18) that Mn-rich pearlite bands have finer carbides and thus form austenite first, and would result in finer areas of segregation in Mn-rich bands and coarser areas in Mn-lean bands.

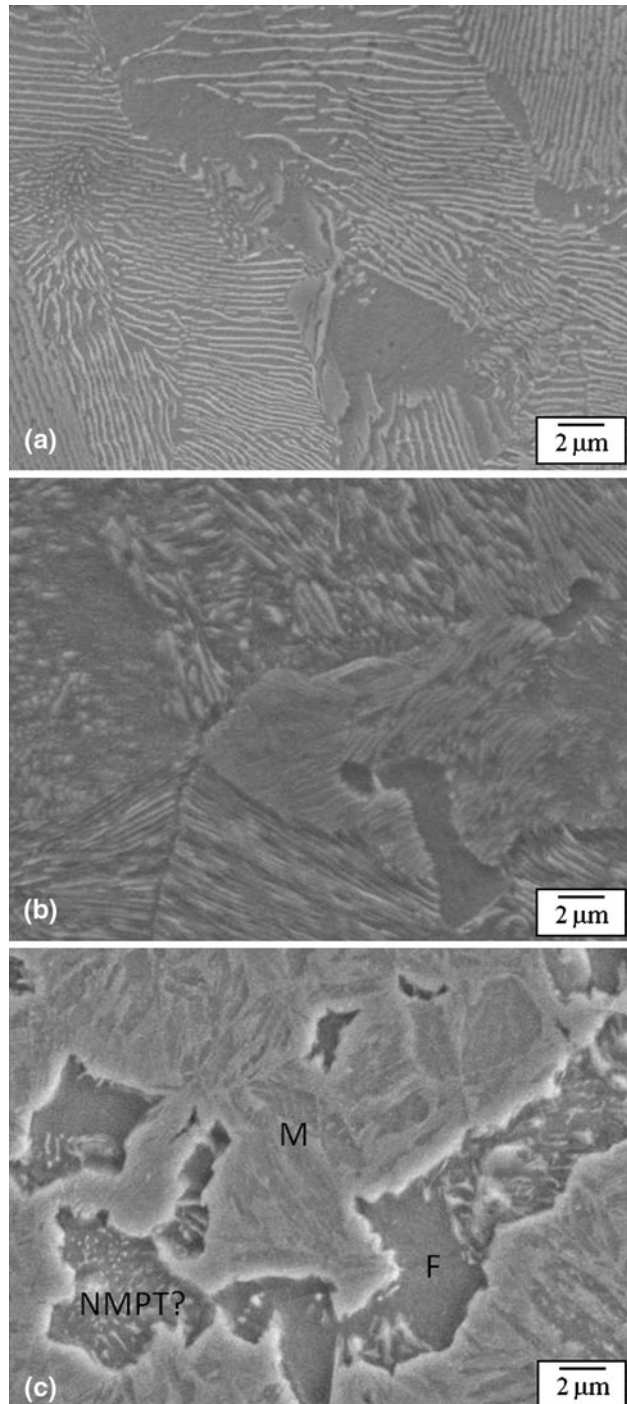


Fig. 5 Final microstructures of 5150 HR samples heated to 750 °C at (a) 30, (b) 3, and (c) 0.3 °C/s followed by immediate He quenching. Electron micrographs. M, martensite; F, ferrite; NMPT, non-martensitic transformation products

3.4 Transformation and Diffusion Simulations

Figure 8 shows results from simulations using DICTRA™, based on initial HR microstructural measurements and assuming local equilibrium. The starting condition with Cr and Mn partitioned to carbide and austenite has been previously documented (Ref 19, 20). The initial partitioned conditions were calculated using Thermo-Calc®.

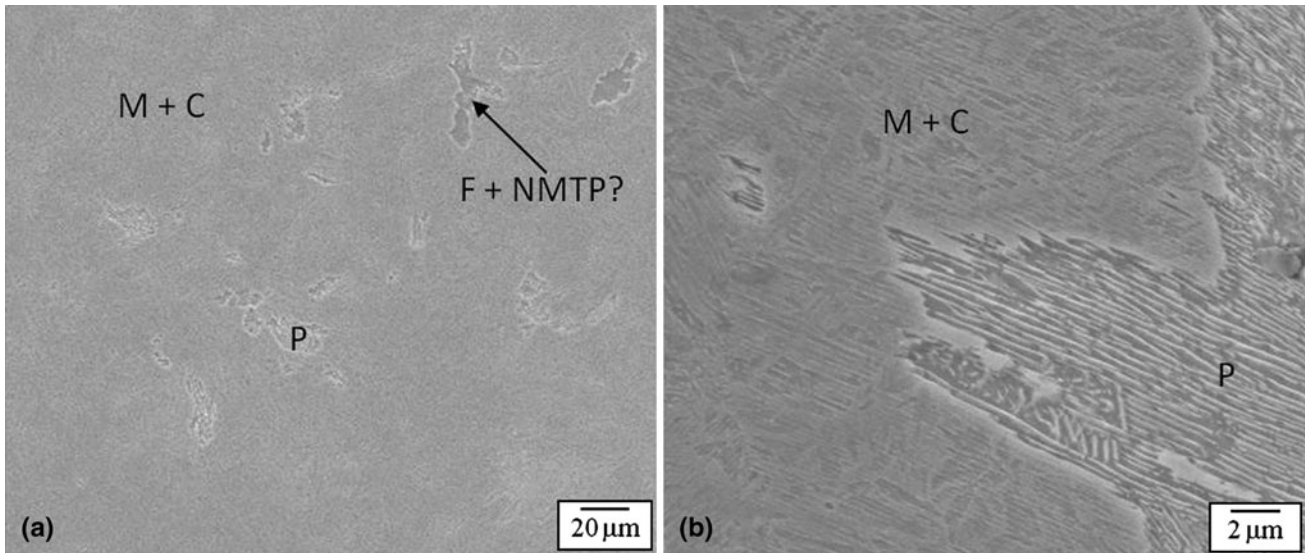


Fig. 6 Final microstructure of the 5150 hot-rolled material after heat treating at 30 °C/s to 775 °C followed by immediate He gas quenching. Electron micrographs. M + C, martensite and cementite; F + NMPT, ferrite and non-martensitic transformation products; P, pearlite

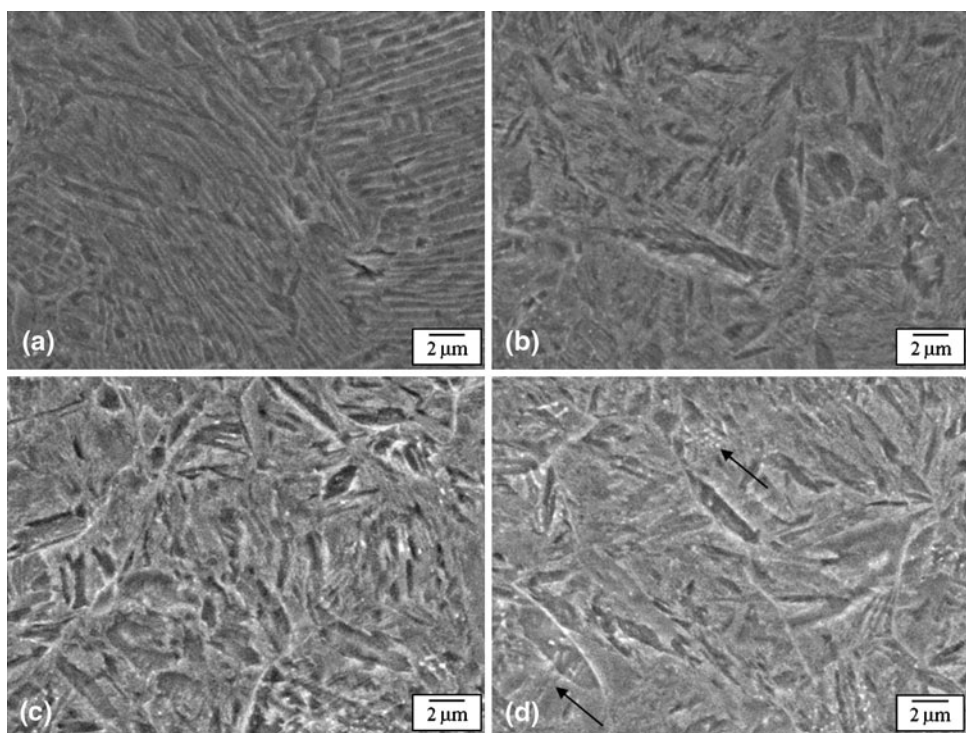


Fig. 7 Final microstructures of the HR material after heat treatment at 300 °C/s to (a) 825 °C, (b) 925 °C, (c) 975 °C, and (d) 1000 °C. Electron micrographs

First, simulations were completed to predict diffusion of alloying elements from cementite lamellae in pearlite, assuming pearlitic ferrite has transformed to austenite. Figure 8(a)-(c) show predicted distributions of C, Cr, and Mn for 300 °C/s heat treatment. They also show that very little carbide is predicted to remain at 1035 °C (i.e., at 1 s), but there would still be significant Cr and Mn segregation. Carbon is nearly evenly distributed in the austenite at all times.

Next, simulations of the proeutectoid ferrite regions, which are last to transform to austenite, were performed. Figure 8(d)-

(f) show results of calculations of proeutectoid ferrite transformation, assuming that prior pearlite regions are fully austenitized. These calculations also predict significant segregation of chromium and manganese with relatively flat carbon distributions. Significant segregation of Cr and Mn may affect the local properties, such as hardenability and corrosion resistance, and further work should be done to examine the practical considerations of this effect. Austenite-ferrite diffusion couple calculation results (presented in Fig. 8d-f) also give predictions for ferrite fraction as a function of time, and are shown in

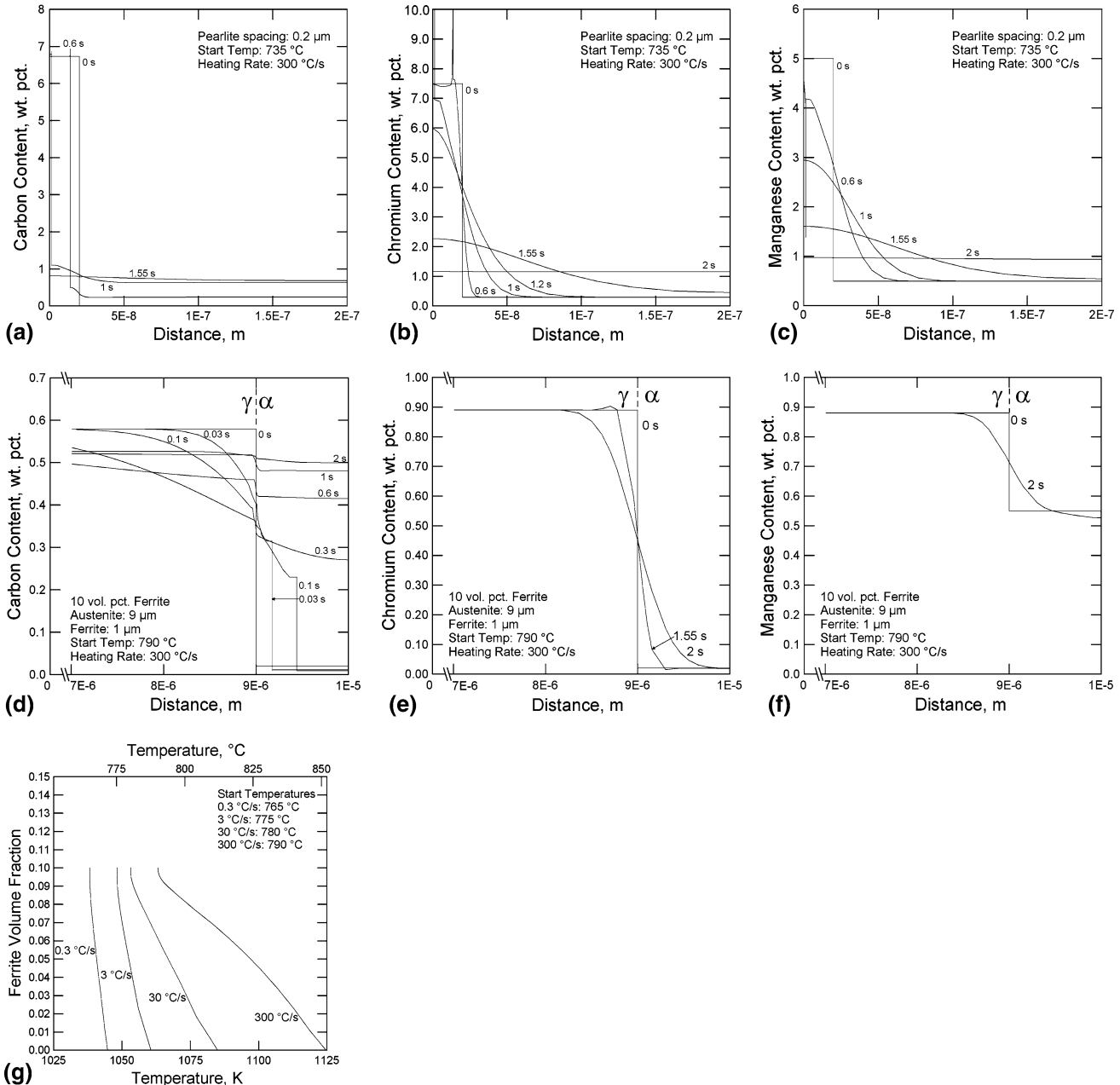


Fig. 8 DICTRA™ diffusion calculation results showing carbon, chromium and manganese distribution for (a-c) the pearlitic cementite dissolution in austenite (cementite on left) and (d-f) the subsequent proeutectoid ferrite-to-austenite transformation. (g) Ferrite fraction as a function of time from DICTRA™ calculations

Fig. 8(g). The temperature at which ferrite disappears is the A_{c3} temperature, which is also plotted in Fig. 3(a). The predicted A_{c3} temperatures from these diffusion simulations are very close to values measured from experimental measurements.

4. Conclusions

Induction hardening heat treatments were studied using dilatometry on 5150 steel with ferrite-pearlite and tempered martensite initial microstructures to assess effects of prior

microstructure and heating rate. The following conclusions can be made:

- On-heating transformation temperatures are significantly higher for a ferrite-pearlite initial microstructure than for a tempered martensite prior microstructure. The difference between the transformation temperatures increases with heating rate.
- Measured maximum hardness is equivalent, independent of starting microstructure, for a given thermal cycle.
- Metallographic evidence indicates significant remnant enrichment of chromium in regions of prior pearlitic

cementite in the ferrite-pearlite initial microstructure. Evidence of alloy segregation was not observed metallographically for the prior tempered martensite microstructure. Further work is necessary to understand the practical implications of local alloy segregation.

- Diffusion-based transformation simulations of induction heat treatment rates support observed ferrite-pearlite alloy segregation, suggest residual alloy segregation is possible for prior tempered martensite, and can be used to tailor austenitization thermal cycles to process requirements. Results are applicable to general induction heating modeling.

Acknowledgments

The authors acknowledge support from the Advanced Steel Processing and Products Research Center, an industry/university cooperative center at the Colorado School of Mines, and Los Alamos National Security, LLC, operator of the Los Alamos National Laboratory under Contract No. DE-AC52-06NA25396 with the US Department of Energy. Sincere thanks to E. Buddy Damm and the Timken Company for supplying experimental materials, Ingo Kurth from Avanel Industries, Inc. for helpful dilatometry discussions, and Mary Van Tyne for invaluable editing support.

References

1. P.M. Unterweiser, *Heat Treater's Guide Standard Practices and Procedures for Steel*, American Society for Metals, Metals Park, OH, 1982
2. J. Orlich, A. Rose, and P. Wiest, *Atlas Zur Wärmebehandlung der Stähle -Band 3, Zeit-Temperatur-Austenitisierung-Schaubilder*, Verlag Stahleisen, M.B.G., Düsseldorf, Germany, 1973
3. Y. Misaka, Y. Kiyosawa, K. Kawasaki, T. Yamazaki, and W.O. Silverthorne, *Gear Contour Hardening by Micropulse Induction Heating System*, Society of Automotive Engineers Document 970971, 1997, p 121–130
4. V. Rudnev, D. Loveless, R. Cook, and M. Black, *Handbook of Induction Heating*, Marcel Dekker, New York, 2003, p 49
5. ASTM E322-07, *Standard Specification for Steel Bars, Alloy, Standard Grades*, Vol 1.05, ASTM International, 2007
6. N. Ridley, A Review of the Data on the Interlamellar Spacing of Pearlite, *Metall. Mater. Trans.*, 1984, **15A**, p 1019–1036
7. H.-S. Yang and H.K.D.H. Bhadeshia, Uncertainties in Dilatometric Determination of Martensite Start Temperature, *Mater. Sci. Technol.*, 2007, **23**, p 556–560
8. ASTM E384-09, *Standard Method for Microindentation Hardness of Materials*, Vol 3.01, ASTM International, 2009
9. ASTM E140-07, *Standard Hardness Conversion Tables for Metals: Relationship Among Brinell Hardness, Vickers Hardness, Rockwell Hardness, Superficial Hardness, Knoop Hardness, and Scleroscope Hardness*, Vol 3.01, ASTM International, 2007
10. G. Krauss, *Steels: Processing, Structure, Performance*, ASM International, Materials Park, OH, 2005, p 60–67
11. R.A. Grange, C.R. Hribal, and L.F. Porter, Hardness of Tempered Martensite in Carbon and Low-Alloy Steels, *Metall. Trans.*, 1977, **8A**, p 1775–1785
12. E. Schmidt, Y. Wang, and S. Sridhar, A Study of Nonisothermal Austenite Formation and Decomposition in Fe-C-Mn Alloys, *Metall. Mater. Trans.*, 2006, **37A**, p 1799–1810
13. M.M. Souza, J.R.C. Guimarães, and K.K. Chawla, Intercritical Austenitization of Two Fe-Mn-C Steels, *Metall. Trans.*, 1982, **13A**, p 575–579
14. G. Molinder, A Quantitative Study of the Formation of Austenite and the Solution of Cementite at Different Austenitizing Temperatures for a 1.27% Carbon Steel, *Acta Metall.*, 1956, **4**, p 565–571
15. D.J. Medlin, G. Krauss, and S.W. Thomson, Induction Hardening Response of 1550 and 5150 Steels with Similar Prior Microstructures, *1st International Conference on Induction Hardening of Gears and Critical Components*, Indianapolis, IN, 1995
16. D.V. Shtansky, K. Nakai, and Y. Ohmori, Pearlite to Austenite Transformation in an Fe-2.6Cr-1C Alloy, *Acta Mater.*, 1999, **47**, p 2619–2632
17. K.D. Clarke, “The Effect of Heating Rate and Microstructural Scale on Austenite Formation, Austenite Homogenization, and As-Quenched Microstructure in Three Induction Hardenable Steels,” Ph.D. thesis, Colorado School of Mines, Golden, CO, USA, 2008
18. D.I. Garcia and A.J. DeArdo, Formation of Austenite in 1.5 Pct Mn Steels, *Metall. Trans.*, 1981, **12A**, p 521–530
19. Z.-K. Liu, L. Höglund, B. Jönsson, and J. Ågren, An Experimental and Theoretical Study of Cementite Dissolution in an Fe-Cr-C Alloy, *Metall. Trans.*, 1991, **22A**, p 1745–1752
20. X.-L. Cai, A.J. Garratt-Reed, and W.S. Owen, The Development of Some Dual-Phase Steel Structures from Different Starting Microstructures, *Metall. Trans.*, 1985, **16A**, p 543–557